Carbon 155 (2019) 506–513

Contents lists available at ScienceDirect

Carbon

journal homepage: www.elsevier.com/locate/carbon

Electromagnetic shielding and multi-beam radiation with high conductivity multilayer graphene film

Chi Fan [a, 1], Bian Wu [a, *], Rongguo Song [b, 1], Yutong Zhao [a], Yahui Zhang [a], Daping He [b, **]

[a] National Key Laboratory of Antennas and Microwave Technology, Shaanxi Joint Key Laboratory of Graphene, Xidian University, Xi'an, 710071, PR China
[b] Hubei Engineering Research Center of RF-Microwave Technology and Application, Wuhan University of Technology, Wuhan, 430070, China

ARTICLE INFO

Article history:
Received 29 July 2019
Received in revised form
26 August 2019
Accepted 6 September 2019
Available online 7 September 2019

ABSTRACT

In the microwave region, graphene material usually has a relatively high resistivity, which limits its application potential in electromagnetic shielding and radiation. Meanwhile, conventional carbon materials are difficult to meet the requirement of electronic devices and electromagnetic shielding in terms of thickness reduction and flexibility. Here, a flexible multilayer graphene film (MGF) with high conductivity and small thickness is achieved by high temperature thermal treatment of GO films and subsequence compression rolling. We experimentally study the EMI shielding performance of the MGF with a thickness of 27 μm, which shows high shielding effectiveness (SE) of 70 dB from 2.6 GHz to 40 GHz. Making use of its high conductivity of 1.13×10^6 S/m and low sheet resistance of 32.7 mΩ/□, a MGF based multi-beam millimeter wave antenna array with average gain of 15.07 dBi and large beam scanning range of 120°is realized for the first time. All the measurements indicate that the flexible, low thickness, low-density and highly conductive multi-layer graphene film have great potential in the application of electromagnetic shielding, electromagnetic conduction and electromagnetic radiation devices.

1. Introduction

Considerable research has been invested to discover new applications of graphene in the THz and infrared portion of the electromagnetic spectrum. In the terahertz and higher frequency bands, graphene's surface conductivity is highly regulated, which makes it well-suited for modulators [1], polarizers [2], plasmonic devices [3–5], photodetectors [6], hyperlenses [7], cloaks [8], absorber [9] and nano-patch antennas [10]. These designs demonstrate the potential of graphene materials to conduct and radiate waves at high frequencies. In the microwave and millimeter wave band, resistivity is the main feature of graphene materials, the use of graphene as a variable resistor is discussed and experimentally characterized by some scholars at microwave and millimeter wave frequencies. For example, some voltage-controlled tunable microwave attenuator based on graphene material is proposed in Refs. [11–17]. Meanwhile, many graphene-based millimeter-wave absorbers are also studied and designed theoretically [18–20]. The resistance property of graphene films is specifically applied in microwave and millimeter wave amplitude modulation devices but it also reflects the low conductivity of graphene materials. Although the surface conductivity of graphene films can be adjusted over 10 times by improving the process, the square resistance still cannot reach single digits [15], which is the major barrier for its applications in conduction and radiation at microwave and millimeter wave. Theoretical prediction suggests that for samples to be significant as microwave antennas, doped multilayer graphene with sheet resistance less than 10 Ω/□ is required [21].

To tackle the electromagnetic pollution problem, considerable efforts have been made for the development of high-performance EMI shielding materials. Lightweight, flexible and high EMI shielding performances are important factors in the selection of shielding materials, which makes carbon-based materials in a dominant position [22–24,35–37]. The total shielding effectiveness (SE) is determined on SE absorption (SEA) and SE reflection (SER). Wentao Zhai et al. [25–27] reported a graphene oxide (GO) film and a graphene G-film, which obtained a shielding effectiveness (SE) of 26.3 dB due to its good SEA. In 2017, Hejun Li et al. [29] reported

* Corresponding author.
** Corresponding author.
E-mail addresses: bwu@mail.xidian.edu.cn (B. Wu), hedaping@whut.edu.cn (D. He).
[1] These authors contributed equally to this work.

https://doi.org/10.1016/j.carbon.2019.09.019
0008-6223/

carbon nanotube–multilayered graphene edge plane core–shell hybrid foam which has a SEA of 21.3 dB and total SE of 47.5 dB. For the carbon material based shielding films, although the conductivity is not a decisive factor of the shielding performance, but the higher conductivity always lends to an excellent SER and finally perfect SE will be obtained. By this way, Shen et al. [25] fabricated the 2000 °C annealed graphene paper showing electrical conductivity of 1×10^4 S/m and SE of 20 dB at 8.4 mm thickness. Zhang et al. [31] fabricated graphene paper synthesized by CVD method, which achieves 1136 S/m and SE of 60 dB at 50 μm thickness. Chao Gao et al. report the synergistic effect of graphene and carbon nanotubes (CNT), that electrical conductivity significant improves from 1.78×10^5 to 2.74×10^5 S/m by adding 20 wt% CNTs into the graphene films, finally, the shielding efficiency of 60 dB from 2 to 18 GHz is obtained [32]. Most recently, *Xi-Xi Wang* et al. construct a 3D eco-mimetic nano architecture for the first time, successfully approaching green and efficient EMI shielding [33]. Besides, they also take some low-dimensional EM functional materials as examples, reveal their crystal and electronic structures, EM response, and energy conversion, as well as their relationship [34,35]. In addition, more work has been done to improve the conductivity of graphene materials [30,36,37,41,42].

In this work, a multi-layer graphene film with high conductivity, which fabricated by high temperature thermal treatment of GO film and subsequence compression rolling are designed. Firstly, we measured the EMI shielding performance of the multi-layer graphene film as EMI shielding film from 2.6 GHz to 40 GHz. Then, a multi-beam array antenna based on multi-layer graphene film, fed by the substrate integrated waveguide butler matrix is fabricated to verify the radiation performance of antenna array based on multilayer graphene film and its connection with metal. To the knowledge of authors, graphene materials were first used as radiation elements connected to a metal feeding network and realized the design of antenna arrays. Finally, the application prospect of this flexible multi-layer graphene with high conductivity in electromagnetic shielding, electromagnetic conduction and electromagnetic radiation is illustrated.

2. Experimental

2.1. Preparation of multi-layer graphene film

The multi-layer graphene film is prepared in the following three steps: Firstly, the GO suspension (purchased from Wuxi chengyi education technology Co. Ltd., the solid content of purchased GO in water is 50%) with the concentration of 10–20 mg/mL was placed in a square die, evaporative drying at room temperature for 24 h, and the GO film was prepared; Then, the GO film was annealed at high temperature of 1300 °C for 2 h and 2800 °C for 1 h, both processes under Ar gas flow, after that the graphene film was fabricated; Finally, the graphene film was rolling compressed under 300 MPa to prepare dense and glossy multi-layer graphene film.

2.2. Characterization

Field emission transmission electron microscope (FETEM) measurements were observed by Talos F200S. Microstructural informations were performed with a JEOL JSM-7610 F Field emission scanning electron microscopy (FESEM). X-ray diffraction (XRD) results were recorded on a Rigaku Smartlab SE instrument using Ni-filtered Cu Ka radiation. Raman spectra patterns were detected by LabRAM HR Evolution Raman Spectrometer.

2.3. Results

Fig. 1a shows the fabrication process of multi-layer graphene film (MGF). Firstly, the GO suspension was diluted to 10–20 g/mL with ultrapure water. In Fig. 1b, the TEM image shows a GO sheet with a size of ~27 μm. The GO suspension was evaporated at room temperature for 24 h, and obtained the GO film. GO film is formed by disorderly stacking of GO sheets and present brown-black color, as shown in Fig. 1c. Then, GO film is carbonized and graphitized during high temperature annealing to form graphene film. Finally, MGF shows glossy surface (Fig. 1d) after rolling compression, which is used to improve the regularity of graphene sheets and the conductivity and density of MGF, as shown in Fig. S1 (Supporting Information). Detailed process can be found in preparation method section. The cross-section SEM image (Fig. 1e) shows the thickness of MGF is ~27 μm and the regular stacking of graphene sheets. In Raman spectroscopy of MGF (Fig. 1f), the small D peak (1335 cm^{-1}) and sharp G peak (1585 cm^{-1}) refers to less lattice defects and the high-level of sp^2 hybridized carbon atoms characteristic. Fig. 1g shows the XRD pattern of MFG. The sharp diffraction peak which locate at 26.5°not only indicates the d (002) is 0.34 nm, but also shows that the graphene layers accumulate more regularly and have longer correlation length due to the high temperature annealing [38]. The diffraction peak (004) exhibits the graphitization structure of MGF is high.

The MGF has good flexibility and can be bent and folded into an airplane, as shown in Fig. 2a. The electrical conductivity of MGF is 1.13×10^6 S/m with the sheet resistance of 32.7 mΩ/□, which test by four-probe method. From Fig. 2b, the resistivity of MGF remains unchanged after 2000 times bending, which further proved that the MGF has good flexibility and mechanical stability.

2.4. EMI shielding measurement

The S parameters (S_{11} and S_{21}) of the samples were measured with Anritsu MS46322A vector network analyzer using the waveguide method from 2.6 GHz to 40 GHz. During the measurement, the foam ($\varepsilon_r = 1$) and the multilayer graphene film attached to the foam (Using foam as a carrier for the samples) were placed in the waveguide to measure its transmission characteristics. The two ports of an Anritsu MS46322A vector network analyzer were connected to the coaxial-waveguide transition, where placed the MGF and foam. The waveguide used for the experiment includes BJ32 (operating frequency form 2.6–3.95 GHz), BJ48 (operating frequency form 3.94–5.99 GHz), BJ70 (operating frequency form 5.38–8.17 GHz), BJ100 (operating frequency form 8.2–12.5 GHz), BJ140 (operating frequency form 11.9–18 GHz), BJ220 (operating frequency form 17.6–26.7 GHz) and BJ320 (operating frequency form 26.3–40 GHz).

The total SE is determined on SEA and SER. The total SE as well as SEA and SER were determined based on the measured S parameters as follows:

$$A = 1–R–T = 1-|S_{11}|^2-|S_{21}|^2 \quad (1)$$

$$SE=SER + SEA = -10\log(1–R)–10\log(T/(1–R)) \quad (2)$$

Where S_{11} is reflection coefficient, S_{21} is transmission coefficient, and A is absorption. To ensure the accuracy of the measurements, two specimens of each sample were selected for testing.

3. Results and discussion

3.1. EMI shielding

Fig. 2a shows a piece of rolled multilayer graphene film, which

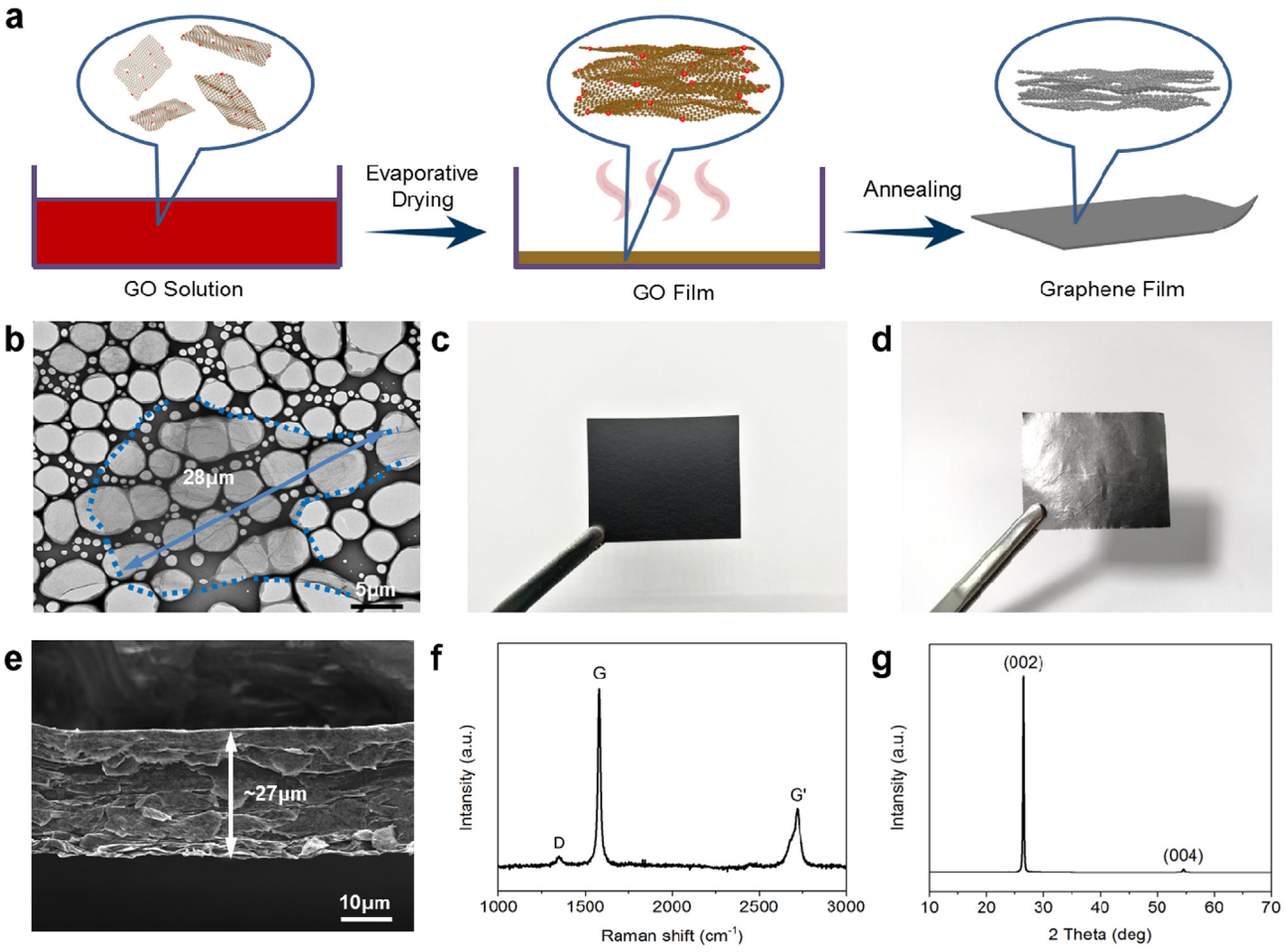

Fig. 1. (a) The fabrication process of MGF; (b) The TEM image of GO sheet; (c) The digital photo of GO film; (d) The digital photo of MGF (e) The SEM image of MGF; (f) Raman spectrum and (g) XRD pattern of a MGF. (A colour version of this figure can be viewed online.)

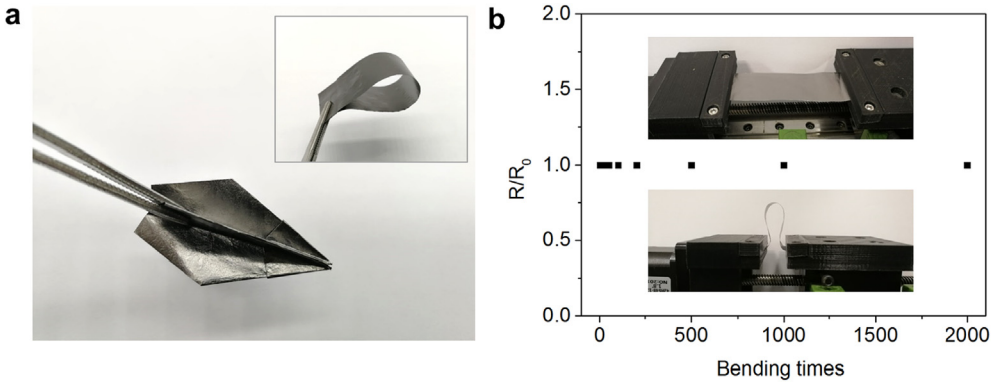

Fig. 2. The flexibility (a) and mechanical stability (b) of MGF. (A colour version of this figure can be viewed online.)

demonstrates that multilayer graphene film have good flexibility and could be fabricated into a variety of shapes and sizes. After that, the samples were cut into different sizes and shapes for EMI shielding measurement by transmission and reflection measurement. In measurement system, rectangular waveguides with length of a and width of b are often used to measure dielectric constant, material loss and shielding effectiveness, which operates in a single mode state as

$$f_{cTE10} < f_0 < f_{cTE20} \tag{3}$$

$$f_{cTEmn} = \frac{c}{2} \times \sqrt{\left(\frac{m}{a}\right)^2 + \left(\frac{n}{b}\right)^2} \tag{4}$$

where TE_{10} is the fundamental mode of the rectangular waveguide and TE_{20} is its first high order mode. Meanwhile, f_0 is the operating

frequency, f_{cTE10} and f_{cTE20} are the cut-off frequency of these two modes respectively. The calculation method of cut-off frequency of rectangular waveguide is also given in formula (4), where c represents the speed of light in vacuum.

Fig. 3a shows the measurement method of rectangular waveguide transmission coefficient and reflection coefficient, and SEA and SER calculated by them. Fig. S2 depicted the measurement samples, foams can be used as a carrier for multilayer graphene films to be measured and two kinds of samples in different thickness are placed separately. To investigate the EMI shielding performance, the S parameters (S_{11} and S_{21}) of the samples were measured with VNA using the waveguide method in a broadband frequency range of 2.6–40 GHz. Four multilayer graphene films were placed in the waveguide for measurement, respectively. According to the results and the electric field distribution in Fig. 3b, when electromagnetic waves pass through the waveguide, the foam has no reflection on the electromagnetic wave but the multilayer graphene film exhibits a strong reflection characteristic, which indicates that it has an excellent electromagnetic interference (EMI) shielding performance. Then, there is almost no wave loss ($1 - |S_{11}|^2 - |S_{21}|^2 \approx 0$), means that $SEA \approx 0$, therefore we can believe that $SER = SE$. After the measurement, some recently reported carbon-based materials and their shielding performances are listed in Table 1.

In general, materials are divided into three categories according to the value of $\sigma/\omega\varepsilon$, $\sigma/\omega\varepsilon \ll 1$: dielectric, $\sigma/\omega\varepsilon \approx 1$: poor conductor, $\sigma/\omega\varepsilon \gg 1$:conductor (σ is the conductivity, ω is the angular frequency and ε is the permittivity). The effect of conductivity on the EMI SE of dielectric is analyzed in Refs. [43–47], the increasing electrical conductivity can enhance the imaginary permittivity, which lead to a higher SE. MGF can be regard as a conductor because of its high conductivity. The electromagnetic field in the conductor can be expressed as

$$E_x = E_0 e^{-(1+j)\alpha z} \tag{5}$$

$$H_y = H_0 e^{-(1+j)\alpha z} \tag{6}$$

since the thickness of MGF is much smaller than the wavelength, the surface impedance of MGF can be expressed as

$$Z_S = E_x/H_y|_{z\approx 0} = E_0/H_0 = \eta_c = (1+j)\sqrt{\omega\mu/2\sigma} = R_S + jX_S \tag{7}$$

where η_c is the wave impedance of conductor, R_S and X_S is the surface resistance and the surface reactance of MGF, respectively. So, the higher the conductivity of a conductor, the smaller the surface impedance and the better the EMI SE performance.

The electrical conductivity of the samples was further measured by using the four-probe method. MGF shows such high electrical conductivity close to metal and has lower thickness and density. Owing to the high conductivity of 1.13×10^6 S/m, it achieves better shielding performances and wider shielding bandwidth than other shielding materials. From the curves in Fig. 3c, we can see that the samples with a thickness of 27 μm shows a high SE of 70 dB and the samples with a thickness of 54 μm shows a higher SE of 80 dB.

3.2. Millimeter wave radiation and beam scanning

In order to further explore the properties of multi-layer graphene film and its performance as an antenna radiator, a kind of unequal amplitude antenna array in the form of chebyshev is designed. Chebyshev array is an antenna array with unequal amplitude distribution, that is, the size of elements in a linear array is different, and each unequal element array forms a linear array through the series feed. The amplitude distribution of different amplitude makes it have lower side lobe level than a uniform linear

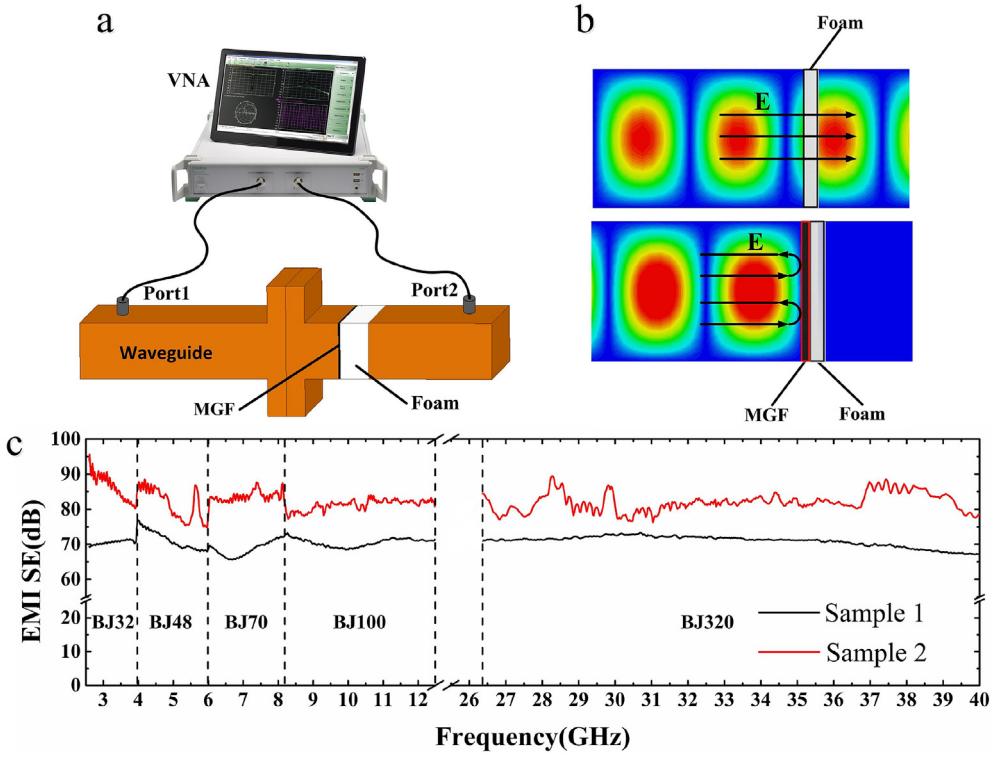

Fig. 3. (a) Measurement method of rectangular waveguide transmission coefficient and reflection coefficient, (b) Electric field distribution of the measured waveguide, (c) SE total in the frequency range of 2.6–40 GHz. (A colour version of this figure can be viewed online.)

Table 1
EMI shielding performances for typical carbon materials.

Ref.	Materials	Thickness [mm]	SE [dB]	Frequency range [GHz]	Density (g*cm-3)	Conductivity [S/m]
[23]	Flexible graphite	3.1	130	1–2	1.1	/
[38]	CF-graphene nonwovens	0.27	28	8–12	0.1	800
[31]	Graphene paper	0.05	60	8–12	/	1136 ± 32
[22]	Graphene Film	0.0084	20	8–12	/	1000
[32]	graphene carbon nanotube	0.015	57.6	2–18	1.45	2.74×10^5
[39]	Graphene aerogel films	1.4	135	0.1–3	0.06	/
[29]	Carbon foam	0.8	24	8.2–12.4	0.0058	/
[25]	graphene foam	0.3	25.2	8.2–59.6	0.06	310
[40]	carbon nanotube	1.8	54.8	8–12	0.01	/
Pro.	MGF	0.025	70	2–40	1.47	1.13×10^6

array, which is convenient for us to observe and measure the main beam direction. As shown in Fig. 4a, an eight-cell chebyshev antenna array based on multilayer graphene film is designed, so as to ensure good transmission between the antenna array and the feeding network, a quarter of the wavelength of the microstrip line needs to be selected for impedance matching (Fig. S3 shows the manufacturing process of FGF antenna array and photograph of the fabricated MGF antenna array which indicated the MGF can be cut into required shapes include arrays).

In order to observe its influence on multi-beam radiation, we choose the Butler matrix as the feeding network of the antenna array. The Butler Matrix is a multi-input, multi-output feeding network that achieves the required bandwidth, scanning power and beamwidth with minimal component count and relatively simple configuration. As it shown in Fig. 4b, butler matrix consists of three basic units, including 3 dB directional couplers, phase shifters, and crossovers. For ease in fabrication, all of these components are geometrically arranged in the same layer. The four feeding ports of Butler matrix are Ports 1–4, and its corresponding output ports connecting to the antenna array are Ports 5–8. Here, when an RF signal is fed into one of the feeding ports, the other feeding ports will be isolated. Besides receiving equal RF signal power (−6 dB) from the feeding port, the four output ports will also exhibit uniform phase differences between adjacent ports. The φ_1 and φ_2 of phase shifters are set at 135° and 0° respectively. The simulation result of this butler matrix is shown in Fig. 4c and d. It can be inferred from these figures that the butler matrix works well in 29–31 GHz. When feeding at any input port, the output signal amplitude of 4 output ports is equal, and the phase difference is stable.

The proposed multi-beam antenna array was fabricated and measured for verification and a multi-beam antenna array base on metal is also fabricated for comparison (Fig. S4). The whole circuit was implemented on F4B substrate with a dielectric constant of 2.2 and a thickness of 0.508 mm, as shown in Fig. 5a and Fig. 5b. So as to accurately measure the various indicators of the array, it is necessary to ensure the accuracy in the production process and the connection method of the two materials. The performance of the antenna array depends on the connection of the multilayer graphene film with the metal and the tightness of the connection

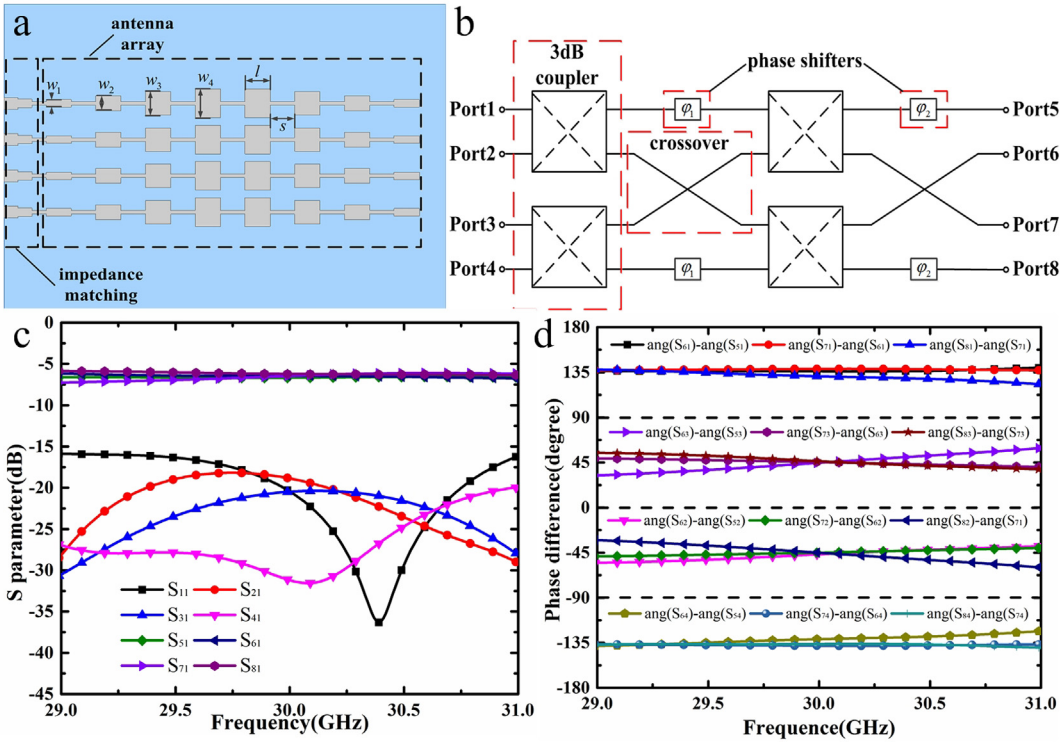

Fig. 4. (a) The structure of antenna array, (b) The block diagram of Butler matrix feeding network, (c) S-parameters of the feeding network, (d) Phase difference of each output port. (A colour version of this figure can be viewed online.)

between the graphene film and dielectric substrate. Simply spread the antenna array based on multilayer graphene film to the dielectric substrate using a temporary spray adhesive (Sulky kk2000), good RF connectivity can be obtained. Next, the metal and the graphene material are glued together with a small amount of conductive adhesive. As a result, the whole multi-beam antenna is finally completed.

When feeding any port, the working state of the antenna can be observed by the surface electric field distribution of the antenna array in Fig. 5c and d. As seen from Fig, 5c, the electromagnetic field of the input port is evenly divided into four channels through the feed network, and each channel has the different phase shift (135, 45, −45,-135, respectively). Then, electromagnetic energy is fed into the antenna array based on MGF. It can been seen from Fig. 5d that the electric field on the 32 antenna elements is distributed symmetrically on the radiating edge, which proves that the antenna array based on MGF are in good radiation condition. The impedance bandwidth and operating frequency of the antenna array are important indicators for measuring the performance of the antenna array. In order to demonstrate the performance of the MGF on a millimeter wave antenna array clearly, a metal antenna of the same size was fabricated for comparison (Fig. S4). It can be seen from Fig. 5e and f that the central frequency of the antenna array is 30 GHz, the graphene antenna array does not produce frequency deviation but it has a wider impedance bandwidth compared with the metal antenna array. That is because antenna array based on MGF have the same size as antenna array based on metal but each MGF antenna unit has a lower Q value than the metal unit, resulting in a wider bandwidth of the overall antenna array ($BW\left(S_{11} \leq 10\text{dB}\right) \approx \frac{1}{\sqrt{2}Q} \times 100\%$). It should be noted that since the antenna structure is symmetrical, so, S_{11}=S_{44} and S_{22}=S_{33}. Last but not least, it should be pointed out that the difference between the measured results and the simulated results in Fig. 5f and e is mainly caused by the machining errors. These errors have only a small impact on the performance of the antenna array, which does not affect our comparison of the overall performance of these two antenna arrays.

To further investigate the performance of MGF antenna array and analyze the radiation beam of it, the radiation pattern and the gain was measured. As exhibited in Fig. 6a and b, it is obvious that the multi-beam antenna array base on MGF has shown wide angle coverage of approximately 120° with good steerable radiation, which indicates that the preset beam scanning ability is completed without beam loss. The gain of antenna array based on MGF and metal are simulated and measured, respectively. As depicted in Fig. 6c and d, in the range of 29–31 GHz, the average gain of the antenna array based on MGF is 15.07dBi. It can be seen that the antenna array based on MGF has a 1.15 dB gain reduction than that based on metal, which is acceptable for an antenna array.

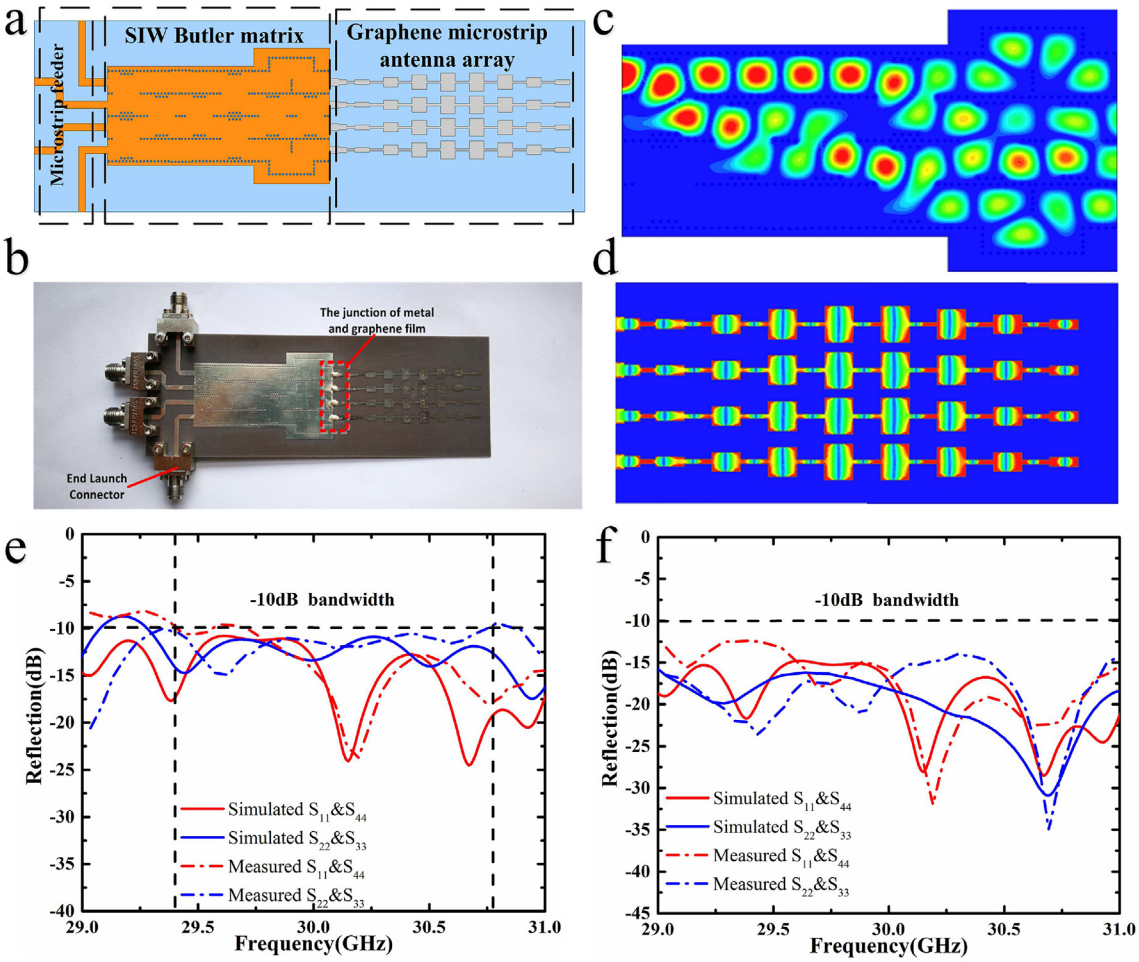

Fig. 5. (a) The structure of the multi-beam antenna array, (b) Photograph of the fabricated multi-beam antenna array based on MGF, (c) Electric field distribution of butler matrix, (d) Electric field distribution of antenna array base on MGF, (e) Simulated and measured reflection of the antenna array based on metal, (f) Simulated and measured reflection of the antenna array based on MGF. (A colour version of this figure can be viewed online.)

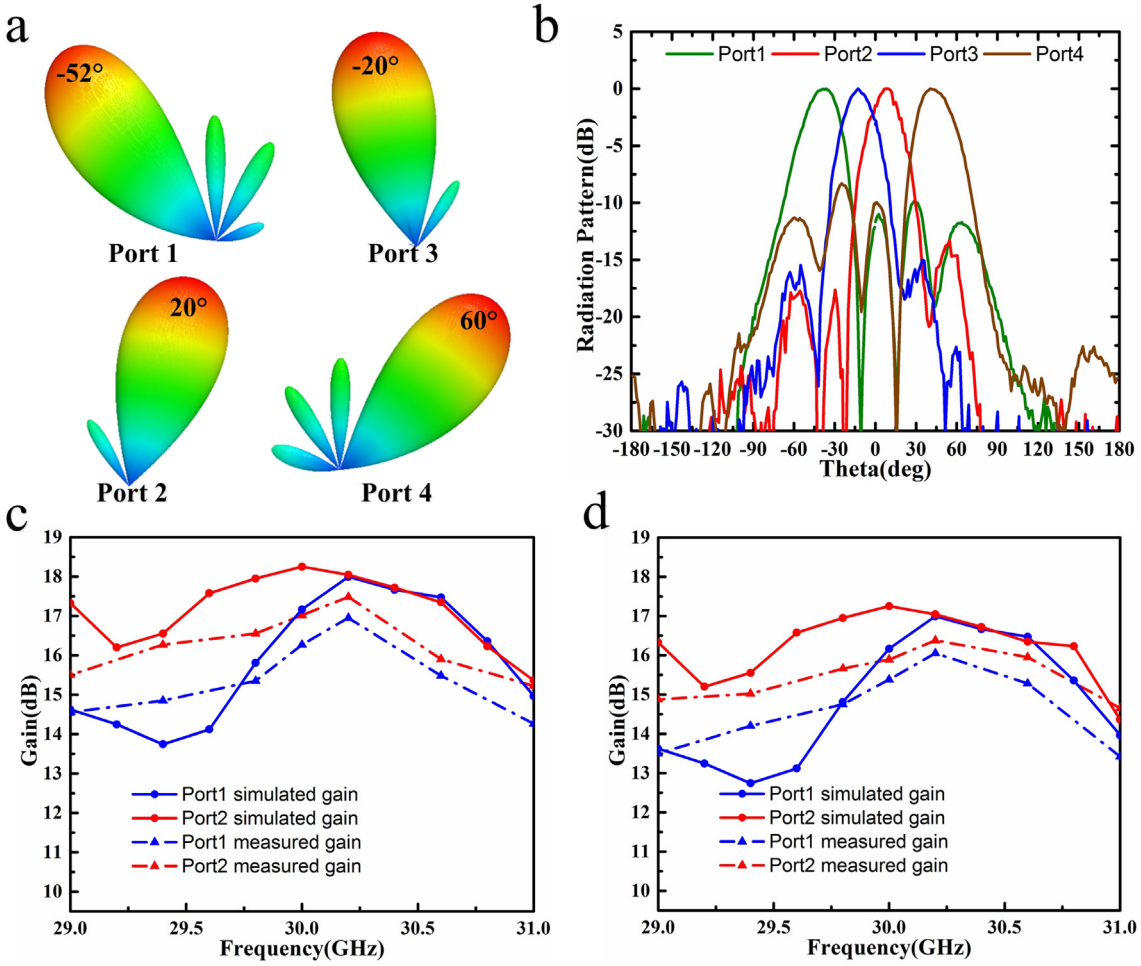

Fig. 6. (a) Simulated antenna pattern, (b) Measured antenna pattern, (c) Gain of the antenna array based on metal, (d) Gain of the antenna array based on MGF. (A colour version of this figure can be viewed online.)

All of the full wave simulations in this paper are solved by ANSYS HFSS V17.0 (High Frequency Structure Simulator) software. Meanwhile, interpolation method was used to solve the S-parameter on the whole operating frequency band, and the solution center frequency was set at 30 GHz.

4. Conclusions

Multilayer graphene films with high conductivity were prepared, and the EMI shielding performance of the multi-layer graphene film from 2.6 GHz to 40 GHz was measured, which achieves a high SE of 70 dB with a thickness of 27 μm and a higher SE of 80 dB with a thickness of 54 μm. Meanwhile, a millimeter-wave multi-beam antenna consisting of a metal-fed network connected to a multilayer graphene radiator is designed and fabricated, which fully demonstrates the potential of this film in electromagnetic radiation devices. Compared with the antenna array based on metal, the bandwidth of the antenna array based on MGF is significantly improved while retaining a wide angle coverage of approximately 120°. Its good space electromagnetic wave reflection ability and high flexibility make it possible to be widely used in conformal antenna and controllable reflector.

Acknowledgements

This work is supported by the National Natural Science Foundation of China under project No.61771360, 61671150, the Shaanxi Youth Science and Technology Star Project No.2017KJXX-32, the key Industry Chain Project of Shaanxi Province No.2018ZDCXL-GY-08-03-01, and the Fundamental Research Funds for the Central Universities.

Appendix A. Supplementary data

Supplementary data to this article can be found online at https://doi.org/10.1016/j.carbon.2019.09.019.

References

[1] M. Liu, X. Yin, E. Ulin-Avila, B. Geng, T. Zentgraf, L. Ju, et al., A graphene-based broadband optical modulator, Nature 474 (2011) 64.
[2] Q. Bao, H. Zhang, B. Wang, Z. Ni, C.H.Y.X. Lim, Y. Wang, et al., Broadband graphene polarizer, Nat. Photonics 5 (2011) 411.
[3] Z. Fei, A.S. Rodin, G.O. Andreev, W. Bao, A.S. McLeod, M. Wagner, et al., Gate-tuning of graphene plasmons revealed by infrared nano-imaging, Nature 487 (2012) 82.
[4] M. Tamagnone, J.S. Gómez-Díaz, J.R. Mosig, Perruisseau-carrier J. Reconfigurable THz plasmonic antenna concept using a graphene stack, Appl. Phys. Lett. 101 (2012) 214102.
[5] L. Ju, B. Geng, J. Horng, C. Girit, M. Martin, Z. Hao, et al., Graphene plasmonics for tunable terahertz metamaterials, Nat. Nanotechnol. 6 (2011) 630.
[6] N.M. Gabor, J.C. Song, Q. Ma, N.L. Nair, T. Taychatanapat, K. Watanabe, et al., Hot carrier–assisted intrinsic photoresponse in graphene, Science 334 (2011) 648.
[7] A. Andryieuski, A.V. Lavrinenko, D.N. Chigrin, Graphene hyperlens for terahertz radiation, Phys. Rev. B 86 (2012) 121108.

[8] P.Y. Chen, A. Alù, Atomically thin surface cloak using graphene monolayers, ACS Nano 5 (2011) 5855.
[9] A. Andryieuski, A. Lavrinenko, Graphene metamaterials based tunable terahertz absorber: effective surface conductivity approach, Opt. Express 21 (2013) 9144.
[10] Z. Xu, X. Dong, J. Bornemann, Design of a reconfigurable MIMO system for THz communications based on graphene antennas, IEEE Trans. Terahertz Sci. Technol 4 (2014) 609.
[11] M. Yasir, S. Bistarelli, A. Cataldo, et al., Enhanced tunable microstrip attenuator based on few layer graphene flakes, IEEE Microw. Wirel. Compon. Lett. 99 (2017) 1.
[12] L. Pierantoni, D. Mencarelli, M. Bozzi, et al., Broadband microwave attenuator based on few layer graphene flakes, IEEE Trans. Microw. Theory Tech. 63 (2015) 2491.
[13] A.Q. Zhang, W.B. Lu, Z.G. Liu, H. Chen, Graphene-Based Dynamically Tunable Attenuator on a half-mode substrate integrated waveguide, Appl. Phys. Lett. 112 (2018) 16.
[14] A.Q. Zhang, W.B. Lu, Z.G. Liu, H. Chen, B.H. Huang, Dynamically tunable substrate-integrated-waveguide attenuator using graphene, IEEE Trans. Microw. Theory Tech. 66 (2018) 3081.
[15] A.Q. Zhang, W.B. Lu, Z.G. Liu, H. Chen, Dynamically tunable attenuator on a graphene-based microstrip line, IEEE Trans. Microw. Theory Tech. 67 (2019) 746.
[16] A.Q. Zhang, W.B. Lu, Z.G. Liu, H. Chen, Graphene-based dynamically tunable attenuator on a coplanar waveguide or a slotline, IEEE Trans. Microw. Theory Tech. 67 (2019) 70.
[17] B. Wu, Y.H. Zhang, H.R. Zu, C. Fan, W.B. Lu, Tunable grounded coplanar waveguide attenuator based on graphene nanoplates, IEEE Microw. Wirel. Compon. Lett. 29 (2019) 330.
[18] D. Yi, X. Wei, Y. Xu, Tunable microwave absorber based on patterned graphene, IEEE Trans. Microw. Theory Tech. 65 (2017) 2819.
[19] D. Yi, X. Wei, Y. Xu, Transparent microwave absorber based on patterned graphene: design, measurement, and enhancement, IEEE Trans. Microw. Theory Tech. 16 (2017) 484.
[20] H. Chen, W.B. Lu, Z.G. Liu, J. Zhang, A.Q. Zhang, B. Wu, Experimental demonstration of microwave absorber using large-area multilayer graphene-based frequency selective surface, IEEE Trans. Microw. Theory Tech. 66 (2018) 3807.
[21] B. Wu, H.M. Tuncer, A. Katsounaros, et al., Microwave absorption and radiation from large-area multilayer CVD graphene, Carbon 77 (2014) 814.
[22] B. Shen, W. Zhai, W. Zheng, Ultrathin flexible graphene film: an excellent thermal conducting material with efficient EMI shielding, Adv. Funct. Mater. 24 (2014) 4542.
[23] X. Luo, D.D.L. Chung, Electromagnetic interference shielding reaching 130 dB using flexible graphite, Carbon 34 (1996) 1293.
[24] W. Huang, L.T. Drzal, Graphene nanoplatelet paper as a light-weight composite with excellent electrical and thermal conductivity and good gas barrier properties, Carbon 50 (2012) 1135.
[25] B. Shen, et al., Microcellular graphene foam for improved broadband electromagnetic interference shielding, Carbon 102 (2016) 154.
[26] Y. Li, B. Shen, D. Yi, et al., The influence of gradient and sandwich configurations on the electromagnetic interference shielding performance of multilayered thermoplastic polyurethane/graphene composite foams, Compos. Sci. Technol. 138 (2017) 209.
[27] B. Shen, Y. Li, D. Yi, et al., Strong flexible polymer/graphene composite films with 3D saw-tooth folding for enhanced and tunable electromagnetic shielding, Carbon 113 (2017) 55.
[29] Q. Song, F. Ye, X. Yin, et al., Carbon nanotube–multilayered graphene edge plane core-shell hybrid foams for ultrahigh-performance electromagnetic-interference shielding, Adv. Mater. 29 (2017) 31.
[30] G. Xin, H. Sun, T. Hu, et al., Large-area freestanding graphene paper for superior thermal management, Adv. Mater. 26 (2014) 4521.
[31] L. Zhang, et al., Preparation and characterization of graphene paper for electromagnetic interference shielding, Carbon 82 (2015) 353.
[32] E. Zhou, J. Xi, Y. Guo, et al., Synergistic effect of graphene and carbon nanotube for high-performance electromagnetic interference shielding films, Carbon 133 (2018) 316.
[33] X.X. Wang, J.C. Shu, W.Q. Cao, M. Zhang, J. Yuan, M.S. Cao, Eco-mimetic nanoarchitecture for green EMI shielding, Chem. Eng. J. 369 (2019) 1068.
[34] M.S. Cao, et al., Electromagnetic response and energy conversion for functions and devices in low-dimensional materials, Adv. Funct. Mater. 29 (2019) 1807398.
[35] M. Zhang, X.X. Wang, W.Q. Cao, J. Yuan, M.S. Cao, Electromagnetic functions of patterned 2D materials for micro–nano devices covering GHz, THz, and optical frequency, Adv. Opt. Mater 7 (2019) 1900689.
[36] C. Teng, D. Xie, J. Wang, et al., Ultrahigh conductive graphene paper based on ball-milling exfoliated graphene, Adv. Funct. Mater. 27 (2017) 1.
[37] L. Peng, Z. Xu, Z. Liu, et al., Ultrahigh thermal conductive yet super flexible graphene films, Adv. Mater. 29 (2017) 1.
[38] W. Song, J. Wang, L. Fan, Y. Li, C. Wang, M. Cao, Interfacial engineering of carbon nanofibere-graphenee-carbon nanofiber heterojunctions in flexible lightweight electromagnetic shielding networks, ACS Appl. Mater 6 (2014) 10516.
[39] J. Xi, Y. Li, E. Zhou, et al., Graphene aerogel films with expansion enhancement effect of high-performance electromagnetic interference shielding, Carbon 135 (2018) 44.
[40] D. Lu, Z. Mo, B. Liang, et al., Flexible, lightweight carbon nanotube sponges and composites for high-performance electromagnetic interference shielding, Carbon 133 (2018) 457.
[41] R.G. Song, Q.L. Wang, B.Y. Mao, et al., Flexible graphite films with high conductivity for radio-frequency antennas, Carbon 130 (2018) 164.
[42] D.L. Tang, Q.L. Wang, Z. Wang, et al., Highly sensitive wearable sensor based on a flexible multi-layer graphene film antenna, Sci. Bull. 63 (2018) 54.
[43] N. Li, Y. Huang, F. Du, et al., Electromagnetic interference (EMI) shielding of single-walled carbon nanotube epoxy composites, Nano Lett. 6 (2006) 1141.
[44] M.S. Cao, W.L. Song, Z.L. Hou, et al., The effects of temperature and frequency on the dielectric properties, electromagnetic interference shielding and microwave-absorption of short carbon fiber/silica composites, Carbon 48 (2010) 788.
[45] B. Wen, M.S. Cao, Z.L. Hou, et al., Temperature dependent microwave attenuation behavior for carbon-nanotube/silica composites, Carbon 65 (2013) 124.
[46] B. Wen, M.S. Cao, M. Lu, et al., Reduced graphene oxides: light-weight and high-efficiency electromagnetic interference shielding at elevated temperatures, Adv. Mater. 26 (2014) 3484.
[47] M.S. Cao, X. Wang, W. Cao, X. Fang, B. Wen, J. Yuan, Thermally driven transport and relaxation switching self-powered electromagnetic energy conversion, Small 14 (2018) 1800987.